

Electromechanically driven chaotic dynamics of voids in metallic thin films

Vivek Tomar, M. Rauf Gungor, and Dimitrios Maroudas*

Department of Chemical Engineering, University of Massachusetts–Amherst, Amherst, Massachusetts 01003-3110, USA

(Received 26 May 2009; revised manuscript received 31 December 2009; published 18 February 2010)

We report a systematic investigation of complex asymptotic states reached in the electromigration-driven morphological evolution of void surfaces in thin films of face-centered cubic metals with $\langle 110 \rangle$ - and $\langle 100 \rangle$ -oriented film planes under the simultaneous action of biaxial tension. The analysis is based on self-consistent dynamical simulations according to a realistic, well-validated, and fully nonlinear model. For $\langle 110 \rangle$ -oriented film planes, we show that upon increasing the applied mechanical stress level, morphologically stable steady states transition to time-periodic states through a subcritical Hopf bifurcation. Further increase in the stress level triggers a sequence of period-doubling bifurcations that sets the driven nonlinear system on a route to chaos. For $\langle 100 \rangle$ -oriented film planes, a transition from steady to time-periodic states also is found to occur at a critical stress level; in this case, the corresponding Hopf bifurcation is supercritical and the nonlinear system is not set on a route to chaos.

DOI: [10.1103/PhysRevB.81.054111](https://doi.org/10.1103/PhysRevB.81.054111)

PACS number(s): 66.30.Qa, 68.35.Ja, 05.70.Ln, 62.20.M–

I. INTRODUCTION

Surface electromigration is an important transport phenomenon that underlies the current-driven morphological evolution of surfaces of electrically conducting and semiconducting solids. Numerous theoretical studies have analyzed the current-driven morphological evolution of metallic surfaces, including surfaces of voids in metallic thin films, without and with the simultaneous action of mechanical stress on the crystalline metal.^{1–24} Among the most intriguing electromigration-induced dynamics on metal surfaces that has been predicted theoretically is the current-driven formation and propagation of various surface wave patterns. These range from current-induced solitary waves and nonlinear surface wave trains propagating on an infinite metal surface in the direction of the electric field,^{12,16} to soliton-like features that travel on large-size void surfaces preceding the failure of metallic thin films,^{8,21} and to stable wave propagation on smaller-size void surfaces in films driven by a stronger-than-critical electric field.^{14,22} Recent theoretical studies also have predicted electromigration-induced complex shape evolution of homoepitaxial islands on electrically conducting substrates¹⁸ and step meandering on vicinal surfaces.²⁰ Fundamental understanding of the nature and origin of such surface wave phenomena and mapping of the surface morphological stability domains associated with the propagation of such wave patterns are crucial for identifying the conditions under which electromechanically driven oscillatory surface dynamics can be generated and stabilized.

In spite of the observation of stable surface wave pattern formation driven by surface electromigration, the extent of complexity that stable surface states can reach in the current-driven morphological evolution of conducting solid surfaces remains largely unexplored. In self-consistent modeling studies of electromigration-driven dynamics of void surfaces in metallic thin films, over a broad range of electric-field strengths, void sizes, and surface transport anisotropy parameters, the most complex asymptotic states that have been stabilized are time-periodic states that consist of surface waves traveling on voids,^{14,22} these morphologically stable

voids are solitons (driven by the electric field) that migrate at a constant speed along the metallic film in the applied-field direction.¹⁷ In addition to these studies, models of electromigration-driven homoepitaxial islands on conducting solid substrate surfaces have been shown to exhibit oscillatory and chaotic dynamics;¹⁸ these are the most complex electromigration-driven stable surface states that have been reported to date. Furthermore, the possibility for a stable complex oscillatory response of metallic surfaces or surface features (including void surfaces and islands on substrates) driven simultaneously by surface electromigration and an additional external force, such as mechanical stress, remains elusive. Exploring such a multiply driven surface morphological evolution is a promising approach toward revealing new intriguing surface dynamics.

Here, we show that geometrically confined surfaces also can exhibit complex morphological response under the simultaneous action of electric fields and mechanical stresses, ranging from time-periodic response to chaotic dynamics. For demonstrating such complex dynamics, we choose to simulate the response of electromechanically driven surfaces of voids in metallic thin films; these voids also can be viewed as surface features analogous to surface pits on solid substrates. Specifically, based on self-consistent dynamical simulations according to a well-validated fully nonlinear model, we study the driven morphological evolution of void surfaces in thin films of face-centered cubic (fcc) metals with $\langle 110 \rangle$ - and $\langle 100 \rangle$ -oriented film planes. For $\langle 110 \rangle$ -oriented film planes, we show that upon increasing the level of the applied mechanical stress, morphologically stable void steady states transition through a subcritical Hopf bifurcation to time-periodic states. Further increase in the stress level sets the driven nonlinear system on a route to chaos through a sequence of period-doubling bifurcations. For $\langle 100 \rangle$ -oriented film planes, we also find that a transition from steady to time-periodic states occurs at a critical stress level. In this case, however, the corresponding Hopf bifurcation is supercritical and the nonlinear system is not set on a route to chaos. Instead, increasing stress starting from a time-periodic state suppresses the oscillatory surface dynamics and leads the void morphology to a stable steady state.

The paper is structured as follows. Section II outlines the fully nonlinear model of void surface morphological evolution used in our analysis, as well as the computational methods employed in our self-consistent numerical simulations of electromechanically driven void dynamics. In Sec. III, the simulation results are presented and the corresponding time-periodic and chaotic asymptotic states are characterized and discussed. Finally, the main conclusions of our study are summarized in Sec. IV.

II. MODEL AND COMPUTATIONAL METHODS

Our analysis of void morphological evolution is based on a continuum model of surface mass transport driven by the simultaneous action of an applied electric field and mechanical stress; the model and accompanying assumptions have been described in detail in Ref. 15. Specifically, the model is implemented in two dimensions on the xy plane of a metallic film of width w along y and extending infinitely along x . The mass transport problem on the void surface is solved self-consistently with the electric- and stress-field distributions in the conducting film that is taken to be elastic and single crystalline. It should be mentioned that although the three-dimensional problem is of interest in practice, it is well beyond the scope of this paper. However, the two-dimensional (2D) case studied here is well validated in the analysis of electromigration-driven void dynamics in metallic thin films. Specifically, a 2D representation is quite satisfactory for voids that extend throughout the film thickness (in z); this is a common type of voids observed in metallic thin films.^{15,25}

In this 2D representation, the morphological evolution of the void surface is governed by the continuity equation, $\partial u_n / \partial t = -\Omega \nabla_s \cdot \mathbf{J}_s$, where u_n is the local displacement normal to the void surface, ∇_s is the surface gradient operator, and \mathbf{J}_s is the total mass flux on the surface expressed by $\mathbf{J}_s = D_s \delta_s [-E_s q_s^* + \nabla_s \mu] \hat{s} / (\Omega k_B T)$. In the flux expression, D_s is the surface atomic diffusivity, Ω is the atomic volume, δ_s / Ω is the number of surface atoms per unit area, E_s is the local electric-field component tangent to the void surface, q_s^* is an effective surface charge, μ is the chemical potential of an atom on the surface, \hat{s} is the local tangent unit vector, k_B is the Boltzmann constant, and T is the temperature. Assuming that the solid responds to stress according to isotropic linear elasticity yields for μ the expression $\mu = \mu_0 - \Omega [(1/2) \text{tr}(\boldsymbol{\sigma} \cdot \boldsymbol{\varepsilon}) - \gamma \kappa]$, where μ_0 is the chemical potential for a flat unstressed surface; γ is the isotropic surface free energy per unit area;¹⁵ $\boldsymbol{\sigma}$ and $\boldsymbol{\varepsilon}$ are the local stress and strain tensors, respectively; and κ is the local surface curvature. The electrostatic problem in the thin film is governed by Laplace's equation for the electrostatic potential. The mechanical deformation of the film's material is governed by Cauchy's mechanical equilibrium equation and is addressed within the framework of isotropic linear elasticity and in the infinitesimal-displacement limit.

Dimensional analysis of the governing equations yields four dimensionless groups: $\Gamma \equiv E_\infty q_s^* w^2 / (\gamma \Omega)$ with E_∞ being the applied electric-field strength that scales the effective electric force with capillary forces, $\Sigma \equiv \sigma_0^2 w / (E \gamma)$ that scales the elastic strain energy with surface energy, a dimensionless

void size $\Lambda \equiv w_i / w$, and the ratio of the principal applied stress components, $R_\sigma \equiv \sigma_{xx} / \sigma_{yy}$ that expresses the anisotropy of the applied stress tensor and determines the state of mechanical stress in the film. In this analysis, $R_\sigma = 1$ and $\sigma_0 > 0$ is the level of the applied biaxial tensile stress. In the above expressions, E is the Young modulus of the material, w is the width of the thin film, and w_i is the initial extent of the void across the film. The resulting diffusional time scale is $\tau \equiv k_B T w^4 / (D_{s,\min} \delta_s \gamma \Omega)$.

In our implementation of the model, we also account for surface diffusional anisotropy through an inhomogeneous surface diffusivity $D_s = D_s(\theta)$, where θ is the angle formed by the applied electric-field direction and \hat{s} . We write $D_s(\theta) = D_{s,\min} f(\theta)$, where $D_{s,\min}$ is the minimum surface diffusivity and $f(\theta) \geq 1$ is an anisotropy function. For fcc metals, such as Al and Cu, we use the functional form $f(\theta) = 1 + A \cos^2[m(\theta + \phi)]$. The dimensionless parameters A , m , and ϕ determine the anisotropy strength, symmetry due to surface crystallographic orientation, and misorientation of a fast surface diffusion direction with respect to the applied electric-field direction, respectively; m is an integer parameter with $m = 1, 2$, and 3 corresponding to $\langle 110 \rangle$ -, $\langle 100 \rangle$ -, and $\langle 111 \rangle$ -oriented film planes. The predictions of the above model with this $f(\theta)$ are in excellent qualitative agreement with experiments of electromigration-induced void morphological evolution in metallic thin films^{8,15} and measurements of electrical resistance evolution in interconnect lines.¹⁹

In an Al film of width $w = 1 \mu\text{m}$, a value of $\Gamma = 50$ corresponds to a current density of about 2 MA/cm^2 , which is typical of accelerated electromigration experiments. For the same film, a value of $\Sigma = 1$ corresponds to a stress of about 140 MPa , which is typical of residual stresses in interconnect lines after cooling and aging.²⁶ We consider this film the "benchmark material system" for this study. The resulting slow time scale for this film at a temperature of 500 K is $\tau \approx 10^4 \text{ h}$; this is an order-of-magnitude estimate based on an approximate value of $D_{s,\min} \delta_s \approx 10^{-24} \text{ m}^3/\text{s}$ for Al at 500 K and $\gamma = 1 \text{ J m}^{-2}$.¹⁵

In the numerical simulations of driven void dynamics, we employ a Galerkin boundary-integral method for the computation of the electrostatic potential Φ and the elastic displacement field \mathbf{u} in conjunction with a front tracking method for monitoring the evolution of the void surface morphology.^{8,15} The boundary-value problems for Φ and \mathbf{u} have been formulated in Ref. 15 and our computational approach has been described in detail in Refs. 8, 15, and 27.

III. TIME-PERIODIC AND CHAOTIC ASYMPTOTIC STATES

A. Low symmetry of surface diffusional anisotropy: $\langle 110 \rangle$ -oriented film planes

At zero stress, $\Sigma = 0$, the numerical simulations of void morphological evolution predict that increasing the electric-field strength Γ , or the void size Λ , or the strength of the diffusional anisotropy A past certain critical values leads to void morphological transitions from steady to time-periodic states.²² The transition onset corresponds to a Hopf bifurcation that may be either supercritical or subcritical, depending

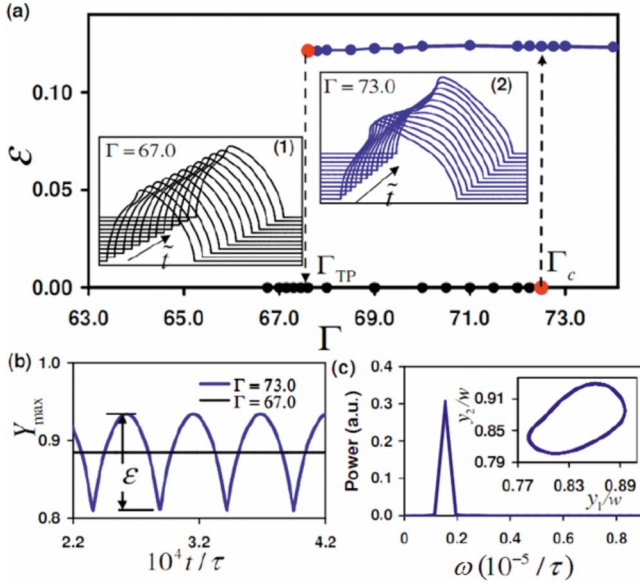


FIG. 1. (Color online) (a) Bifurcation diagram of the electromigration-driven surface morphological response of a void in a metallic thin film. The oscillation amplitude ε in the evolution of the maximum extent of the void surface across the film, Y_{\max} , is plotted at the asymptotic state as a function of the electric-field strength Γ . Solid black and dark gray (blue online) circles denote steady and time-periodic states, respectively. The other parameter values are $\Sigma=0$, $\Lambda=0.61$, $A=10$, $m=1$, and $\phi=90^\circ$. At $\Gamma=\Gamma_c$, a subcritical Hopf bifurcation occurs leading to hysteresis and stable asymptotic-state multiplicity and at $\Gamma=\Gamma_{TP}$ the bifurcating time-periodic branch turns around and gains stability. Insets (1) and (2) show sequences of configurations in the evolution of the void morphology at the asymptotic states for $\Gamma=67.0$ (steady state) and $\Gamma=73.0$ (time-periodic state), respectively; in inset (2), void morphologies are shown over a time interval that corresponds to one time period. (b) Evolution of Y_{\max} at the asymptotic states for $\Gamma=67.0$ (steady state) and $\Gamma=73.0$ (time-periodic state). (c) Power spectrum of the time-periodic state shown in (b); the corresponding phase portrait is shown in the inset.

on the symmetry of the surface diffusional anisotropy as determined (through m) by the crystallographic orientation of the film plane.²² In this section, the focus is on $m=1$, where the $\Sigma=0$ Hopf bifurcation is subcritical. Figure 1(a) is the bifurcation diagram with Γ as the bifurcation parameter and the other parameters fixed (at $\Sigma=0$, $\Lambda=0.61$, $A=10$, $m=1$, and $\phi=90^\circ$); the plotted morphological norm ε corresponds to the oscillation amplitude and is defined in Fig. 1(b). At the Hopf point $\Gamma=\Gamma_c$, the steady state ($\varepsilon=0$) loses stability, but the bifurcating time-periodic branch is unstable until it turns around at $\Gamma=\Gamma_{TP}<\Gamma_c$ and becomes stable with an oscillation amplitude $\varepsilon>0$. $\Gamma_c\approx 72$, which corresponds to a current density of ~ 3 MA/cm² in the benchmark material system; this is on the same order of magnitude with the typical current density in accelerated electromigration experiments. The subcritical bifurcation causes hysteresis, which results in two stable asymptotic states (one steady and one time periodic) over a range of Γ .

Representative results for the void surface morphological evolution at different values of Γ are shown in insets (1) and

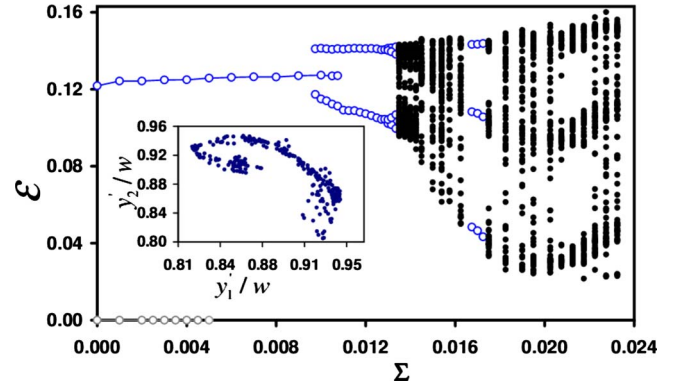


FIG. 2. (Color online) Bifurcation diagram of the electromechanically driven surface morphological response of a void in a metallic thin film showing a period-doubling-bifurcation route to chaos. The oscillation amplitude ε in the evolution of Y_{\max} at the asymptotic state is plotted as a function of the stress level Σ . The other parameter values are $\Gamma=68.0$, $\Lambda=0.61$, $A=10$, $m=1$, and $\phi=90^\circ$. Gray and dark gray (blue online) open circles denote steady and time-periodic states, respectively, while black solid circles denote chaotic response. The inset shows the Poincaré section of the chaotic attractor on the 2D phase plane for $\Sigma=0.0145$.

(2) of Fig. 1(a). The evolution depicted in inset (1) shows a steady state at $\Gamma=67.0<\Gamma_c$; the stable void shape is steady and migrates along the film (in x) at a constant speed. This morphologically stable void translating along x at a constant speed corresponds to a solitary wave. The evolution depicted in inset (2) shows a time-periodic state at $\Gamma=73.0>\Gamma_c$; the void is stable and migrates along the film at a constant speed (solitary wave), but there is also a wave traveling along the void surface (shown as a traveling surface protrusion) that determines the maximum extent of the void surface across the film, $y_{\max}(t)$. This is evident in Fig. 1(b) that depicts the evolution of $Y_{\max}\equiv y_{\max}/w$ for the two asymptotic states at $\Gamma=67.0$ and 73.0 . The power spectrum $P(\omega)$ of the Y_{\max} evolution for $\Gamma=73.0$ is shown in Fig. 1(c) and exhibits a single frequency, the one that characterizes the time-periodic morphological response; $P(\omega)$ expresses the distribution of frequencies in the Fourier time-series representation of the periodic orbit and is generated by fast Fourier transform of $Y_{\max}(t)$ at the asymptotic state. The inset of Fig. 1(c) depicts the corresponding phase portrait of this limit cycle, namely, a 2D phase-plane trajectory on a plane defined by the y coordinates, y_1 and y_2 , of two points on the void surface given by two specific non-neighboring nodes in the surface discretization near the void tip.

Starting from the response expressed by the bifurcation diagram in Fig. 1(a), we perturb this driven dynamical system through the simultaneous application of biaxial tensile stress for further exploration of complexity in the void surface morphological response. Specifically, from the stable steady region of this hyperplane in parameter space ($\varepsilon=0$, $\Sigma=0$, $\Gamma<\Gamma_c$), we move along the Σ axis with $\Sigma>0$. The resulting dynamical response predicted by our numerical simulations is intriguing and is summarized in the bifurcation diagram of Fig. 2 with Σ as the bifurcation parameter, $\varepsilon=\varepsilon(\Sigma)$, for $\Gamma=68.0$, and the other parameters (Λ , A , m , and ϕ) kept equal to those that yielded the results of Fig. 1(a). As

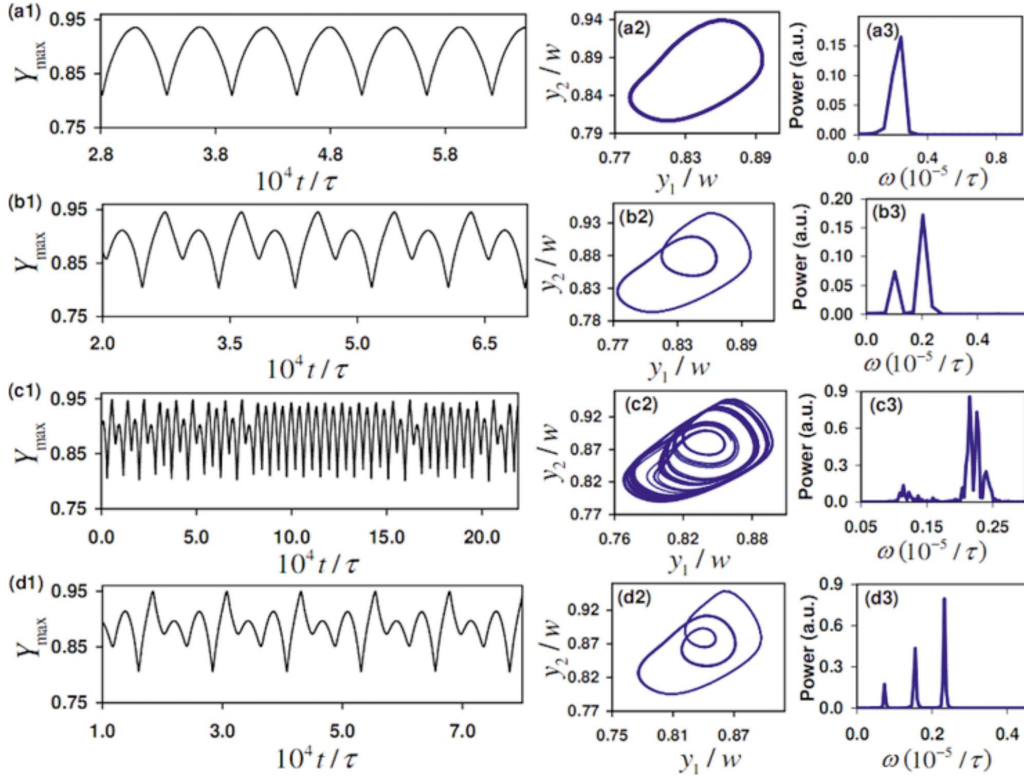


FIG. 3. (Color online) Complex oscillatory states in the dynamics of an electromechanically driven void in a metallic thin film under biaxial tension with increasing mechanical stress level Σ . (a1), (b1), (c1), and (d1) Evolution of the maximum extent of the void surface across the metallic thin film, Y_{\max} , at the asymptotic state; (a2), (b2), (c2), and (d2) the corresponding phase portraits; and (a3), (b3), (c3), and (d3) the corresponding power spectra for parameters $A=10$, $m=1$, $\phi=90^\circ$, $\Lambda=0.61$, and $\Gamma=68.0$. (a1)–(a3) depict a time-periodic state with a single period for $\Sigma=0.005$; (b1)–(b3) depict a time-periodic state with two periods for $\Sigma=0.012$; (c1)–(c3) depict a chaotic state for $\Sigma=0.0145$; and (d1)–(d3) depict a time-periodic state with three periods for $\Sigma=0.01675$, which lies in a periodic window between two chaotic regimes.

Σ increases from $\Sigma=0$, a Hopf bifurcation occurs at $\Sigma=\Sigma_{c,1}$ leading to a stable time-periodic response from a stable steady one. $\Sigma_{c,1}\approx 0.005$, which corresponds to a stress level on the order of 10 MPa in the benchmark material system; this is lower by one order of magnitude than the typical residual stress level in interconnects. This Hopf bifurcation also is subcritical, resulting in hysteresis and multiplicity of stable asymptotic states (one steady and one time-periodic state) over a narrow Σ range. As in the absence of stress (Fig. 1), the time-periodic response is characterized by a protrusion on the void surface that travels along the surface, while the void itself is a soliton that translates along the film in the electric-field direction at a constant speed. As Σ increases beyond a second critical stress level, $\Sigma=\Sigma_{c,2}$, a period-doubling bifurcation is triggered. At this bifurcation point, the time-periodic (period-1) state loses stability and a period-2 state bifurcates from the period-1 state; this period-2 time-periodic state is a periodic solution characterized by two fundamental frequencies and two amplitudes and resulting in two wave modes traveling simultaneously on the void surface. This period-doubling bifurcation also is subcritical and the period-2 state becomes stable only after it turns around, which leads to hysteresis with two stable periodic states, a period-1 and a period-2, over a much narrower Σ range. Further increase in Σ leads to another period-

doubling bifurcation giving rise to a period-4 solution with four fundamental frequencies and four amplitudes; this trend continues upon increasing Σ , triggering a sequence of period-doubling bifurcations.

This sequence of bifurcations sets the doubly driven dynamical system on a route to chaos, as Σ increases for given Γ , Λ , and surface diffusional anisotropy parameters A , m , and ϕ . In Fig. 2, two chaotic regimes are evident separated by a time-periodic window. This periodic window exhibits a period-3 solution with three fundamental frequencies and three amplitudes, a 3-cycle; as Σ increases, this periodic solution brings the system again to chaos through another sequence of period-doubling bifurcations. This chaotic state is characteristic of the void morphological response until Σ becomes high enough to cause the failure of the film, i.e., extension of the void tip until it touches the opposite edge of the film.

The characteristics of the complex oscillatory asymptotic states over the range of Σ examined are shown in Fig. 3 for an increasing level of mechanical stress. Specifically, the evolution of the maximum extent of the void surface across the metallic thin film is depicted together with the corresponding phase portraits and power spectra for the parameter set (Γ , Λ , A , m , and ϕ) that yielded the bifurcation diagram of Fig. 2 at $\Sigma=0.005$ [Fig. 3, (a1)–(a3)], $\Sigma=0.012$ [Fig. 3,

(b1)–(b3)], $\Sigma=0.0145$ [Fig. 3, (c1)–(c3)], and $\Sigma=0.01675$ [Fig. 3, (d1)–(d3)]; the asymptotic states depicted are a period-1, a period-2, a chaotic, and a period-3 state in the periodic window between the two chaotic regimes of Fig. 2, respectively. The chaotic state of Fig. 3, (c1)–(c3) is characterized by an irregular or aperiodic trajectory with a continuous spectrum of oscillation frequencies and amplitudes. This strange attractor has a fractal dimension, which was determined by generating the Poincaré section of the trajectory on the 2D phase plane; for $\Sigma=0.0145$, this Poincaré section is depicted in the inset of Fig. 2. A box counting technique²⁸ was applied to calculate the capacity dimension of the chaotic attractors. For the chaotic attractor of Fig. 3(c), the zeroth-order capacity dimension $d^{(0)}$ was found to be $d^{(0)}=1.20\pm 0.05$; $d^{(0)}=\lim_{\delta\rightarrow 0}[\ln(1/n)/\ln(\delta)]$, where n is the number of square boxes to fully capacitate the Poincaré section and δ is the size (side length) of the boxes. For the two chaotic regimes of Fig. 2, the computed mean values of $d^{(0)}$ ranged from 1.15 to 1.25.

We explored systematically the complex asymptotic states reached in the electromechanically driven void dynamics with Σ as the bifurcation parameter over a broad range of applied electric-field strength Γ , including $\Gamma_{\text{TP}}<\Gamma<\Gamma_c$, as well as $\Gamma<\Gamma_{\text{TP}}$ and $\Gamma>\Gamma_c$. In all cases, the dynamical response is consistent with that depicted in Figs. 2 and 3 (for $\Gamma=68.0$, i.e., $\Gamma_{\text{TP}}<\Gamma<\Gamma_c$): upon increasing Σ , a sequence of period-doubling bifurcations sets the system on a route to chaos, the system exits the chaotic regime into a time-periodic state characterized by three periods, and another sequence of period-doubling bifurcations takes the system out of this periodic window and into a second chaotic regime prior to film failure. Figure 4(a) shows a representative bifurcation diagram, $\varepsilon=\varepsilon(\Sigma)$, for $\Gamma=66.0<\Gamma_{\text{TP}}$ and parameters Λ , A , m , and ϕ equal to those that yielded the results of Figs. 1(a) and 2. Changes in Γ result in different critical values of Σ for the various bifurcation points, differences in the widths of the periodic windows, as well as different asymptotic-state multiplicities over a Σ range due to the hysteresis caused by each of the subcritical bifurcations. For example, Fig. 4(a) exhibits a narrow Σ range before the Hopf point is reached ($\Sigma<\Sigma_{c,1}$), over which three stable asymptotic states are possible: a steady, a period-1, and a period-2 state; this is different from the response of Fig. 2 at $\Sigma<\Sigma_{c,1}$. Figure 4(b) shows the dependence on Γ of the critical stress levels for the subcritical Hopf bifurcation and the first period-doubling bifurcation, $\Sigma_{c,1}$ and $\Sigma_{c,2}$, respectively; for $\Gamma>\Gamma_c$, i.e., beyond the $\Sigma=0$ Hopf point, no steady states are stabilized. $\Sigma_{c,1}(\Gamma)$ and $\Sigma_{c,2}(\Gamma)$ are shown to be monotonically decreasing and monotonically increasing, respectively. Consequently, the difference $\Sigma_{c,2}-\Sigma_{c,1}$ is a monotonically increasing function of Γ over the proper Γ range, $\Gamma<\Gamma_c$, as shown in Fig. 4(c).

B. High symmetry of surface diffusional anisotropy: $\langle 100 \rangle$ -oriented film planes

In addition to the systematic investigation of electromechanically driven void dynamics for $m=1$, the possibility for complex oscillatory asymptotic states also was examined in

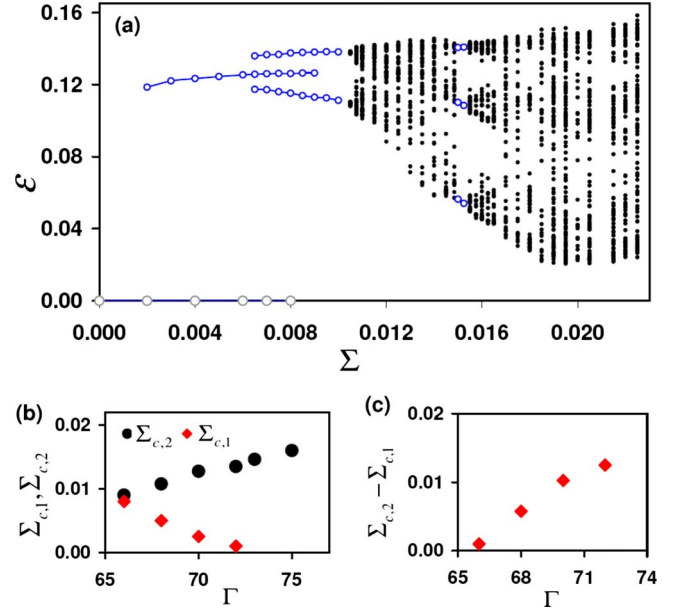


FIG. 4. (Color online) (a) Bifurcation diagram of the electromechanically driven surface morphological response of a void in a metallic thin film showing a period-doubling-bifurcation route to chaos. The oscillation amplitude ε in the evolution of Y_{max} at the asymptotic state is plotted as a function of the stress level Σ . The other parameter values are $\Gamma=66.0$, $\Lambda=0.61$, $A=10$, $m=1$, and $\phi=90^\circ$. Gray and dark gray (blue online) open circles denote steady and time-periodic states, respectively, while black solid circles denote chaotic response. (b) Dependence on the electric-field strength Γ of the critical stresses $\Sigma_{c,1}$ (black solid circles) and $\Sigma_{c,2}$ [light gray (red online) solid diamonds] at the Hopf and first period-doubling-bifurcation points, respectively, for parameter values $\Lambda=0.61$, $A=10$, $m=1$, and $\phi=90^\circ$. (c) Dependence on Γ of $\Sigma_{c,2}-\Sigma_{c,1}$.

the case of higher symmetry of surface diffusional anisotropy, $m=2$, i.e., for $\langle 100 \rangle$ -oriented film planes, based on numerical simulations of doubly driven void morphological evolution. In this symmetry case, Fig. 5(a) shows a representative bifurcation diagram, where the morphological norm ε is plotted as a function of the electric-field strength Γ , which is the corresponding bifurcation parameter; the other parameters are fixed at $\Sigma=0$, $\Lambda=0.80$, $A=2.9$, $m=2$, and $\phi=45^\circ$. In the absence of mechanical stress, $\Sigma=0$, in a manner similar to the case $m=1$, the void morphological response transitions from a steady state to a time-periodic state when the electric-field strength is increased beyond a critical value, $\Gamma=\Gamma_c$, through a Hopf bifurcation. It should be mentioned that, similar to the case $m=1$, the steady state refers to a stable steady void morphology that translates along the film in the applied electric-field direction; in other words, the migrating void is a solitary wave that can be viewed as a steady state in a frame of reference moving at the constant void migration velocity. Contrary to the case $m=1$, however, the Hopf bifurcation is supercritical in this case. Representative results for the void surface morphological evolution at the time-periodic asymptotic state are shown in Fig. 5(b); the evolution is characterized by a surface wave traveling on the surface of a stable void that is migrating along the film at a

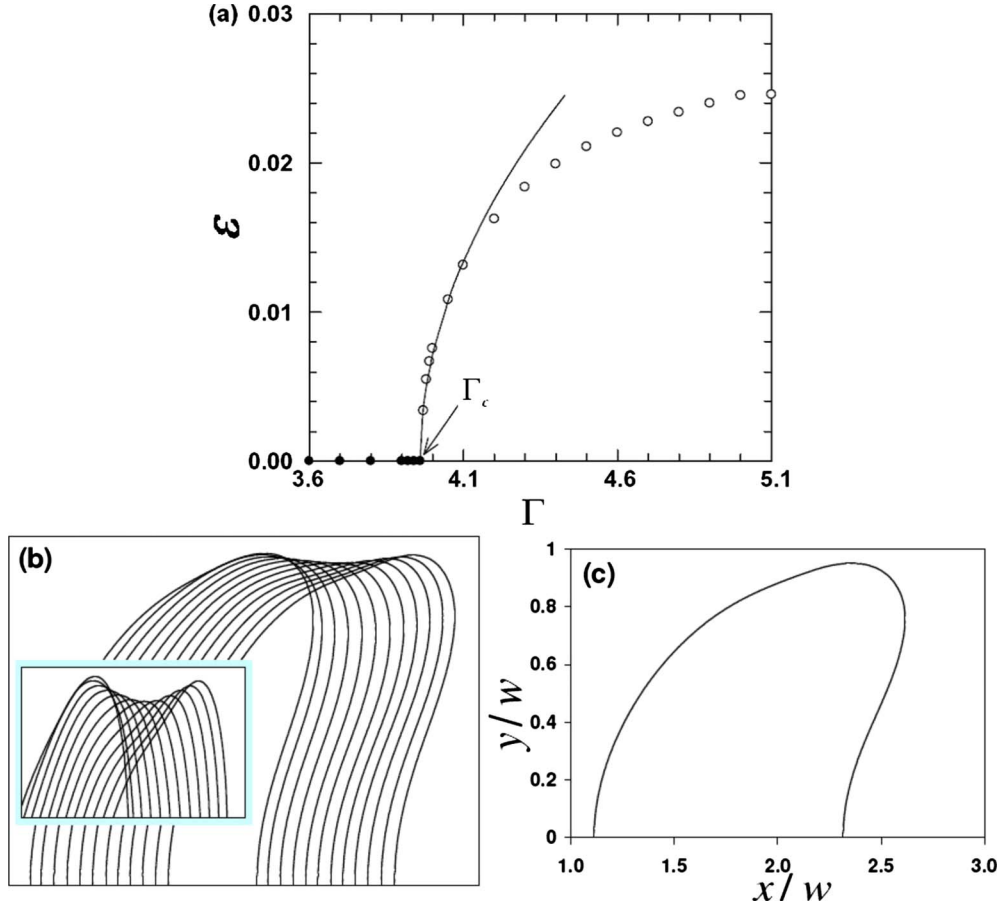


FIG. 5. (Color online) (a) Bifurcation diagram of the electromigration-driven surface morphological response of a void in a metallic thin film. The oscillation amplitude ε in the evolution of the maximum extent of the void surface across the film, Y_{\max} , is plotted at the asymptotic state as a function of the electric-field strength Γ . Solid and open circles denote steady and time-periodic states, respectively. The solid curve is a quadratic polynomial fit to the parametric dependence of the stable time-periodic response in the vicinity of criticality, $\Gamma \rightarrow \Gamma_c^+$. The other parameter values are $\Sigma=0$, $\Lambda=0.80$, $A=2.9$, $m=2$, and $\phi=45^\circ$ (taken from Ref. 22). (b) Sequences of configurations in the evolution of the void morphology at the asymptotic state for $\Gamma=4.05$. The inset in (b) depicts close views of the configurations in the evolution sequence in the vicinity of the void tip. (c) A void configuration from the morphological evolution sequence shown in (b).

constant speed. The traveling surface wave is evident in Fig. 5(b), especially in the close view of the void-tip evolution sequence shown in the inset. A void configuration at the time-periodic asymptotic state is depicted in Fig. 5(c); comparison of this void morphology with those in the inset of Fig. 1(a) emphasizes the morphological differences of the time-periodic states at $\Gamma > \Gamma_c$ and $\Sigma=0$ in the two symmetry cases, $m=2$ and 1, respectively.

For the study of electromigration-driven void dynamics under the simultaneous action of mechanical stress, in this symmetry case, $m=2$, the same approach was followed as in the case $m=1$. Starting from the response expressed in the bifurcation diagram in Fig. 5(a), the driven nonlinear system is perturbed by the application of biaxial tensile stress. Specifically, from the stable time-periodic region of the hyperplane of Fig. 5(a) in parameter space ($\varepsilon > 0$, $\Sigma=0$, $\Gamma > \Gamma_c$), we moved along the Σ axis by increasing the strength of the applied biaxial tensile stress ($\Sigma > 0$). The resulting dynamical response is summarized in the bifurcation diagram in Fig. 6(a) with Σ as the bifurcation parameter, $\varepsilon = \varepsilon(\Sigma)$, for $\Gamma=4.05$, and the other parameters (Λ , A , m , and ϕ) kept equal to those that yielded the results of Fig. 5(a). At

low stress levels, the void morphological response reaches a stable time-periodic asymptotic state. At a critical stress level, $\Sigma = \Sigma_c$, a bifurcation occurs that marks the onset of transition from the time-periodic states to steady states. This corresponds to a Hopf bifurcation at $\Sigma = \Sigma_c$ as the stress level decreases from higher values of Σ . Contrary to the case $m=1$ and consistently with the $\Sigma=0$ bifurcation in $\varepsilon(\Gamma)$ at $m=2$, this Hopf bifurcation is supercritical. This is confirmed by the quadratic polynomial fit, $\Sigma = \Sigma_c - B\varepsilon^2$, where B is a constant, to the parametric dependence [$\varepsilon = \varepsilon(\Sigma)$], of the stable time-periodic response in the vicinity of criticality, $\Sigma \rightarrow \Sigma_c^-$ (i.e., for $0 < \Sigma < \Sigma_c$); this parametric dependence is consistent with supercritical Hopf bifurcation theory.²⁹ This implies that, for $m=2$, the applied biaxial mechanical stress suppresses the surface-electromigration-induced time-periodic void morphological response, which is characterized by a protrusion on the void surface (a soliton-like feature) that travels along the surface of the void that is translating along the film at a constant speed. For $\Sigma > \Sigma_c$, and for the same values of the other parameters (Γ , Λ , A , m , and ϕ), the void translates along the metallic film with a stable steady shape at a constant speed. After a certain stress level, how-

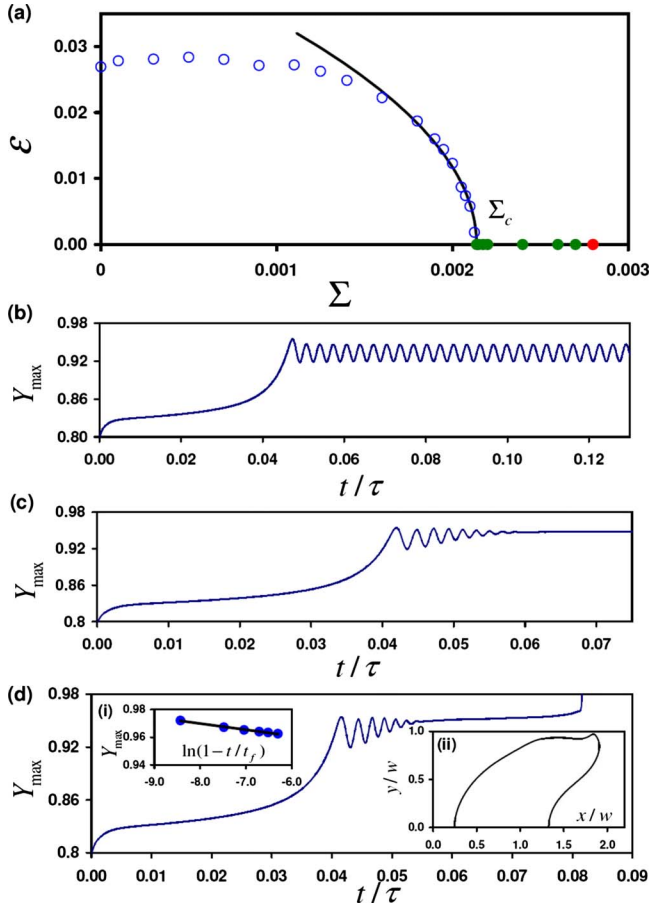


FIG. 6. (Color online) (a) Bifurcation diagram of the electromechanically driven surface morphological response of a void in a metallic thin film. The oscillation amplitude ε in the evolution of the maximum extent of the void surface across the film, Y_{\max} , is plotted at the asymptotic state as a function of the applied mechanical stress Σ . Open dark gray (blue online) and solid light gray (green online) circles denote time-periodic and steady states, respectively. The gray (red online) solid circle marks the onset of film failure. The solid curve is a quadratic polynomial fit to the parametric dependence of the stable time-periodic response in the vicinity of criticality, $\Sigma \rightarrow \Sigma_c^-$. The other parameter values are $\Gamma=4.05$, $\Lambda=0.80$, $A=2.9$, $m=2$, and $\phi=45^\circ$. (b) and (c) Evolution of Y_{\max} toward or at the asymptotic states for $\Gamma=4.05$ and (b) $\Sigma=0.0$ and (c) $\Sigma=0.026$. (d) Evolution of Y_{\max} at $\Gamma=4.05$ and $\Sigma=0.028$. The corresponding asymptotic state (a steady state) is unstable and failure occurs by void-tip extension to reach the opposite edge of the film. Inset (i) shows Y_{\max} as a function of $\ln(1-t/t_f)$ near failure, where t_f is the time to failure; the solid line is a linear fit to the dependence of Y_{\max} on $\ln(1-t/t_f)$. Inset (ii) shows a snapshot from the void evolution prior to failure.

ever, the applied mechanical stress destabilizes this steady state; the instability leads to failure of the film, facilitated by the fast extension of the void tip to reach the opposite edge of (and, therefore, sever) the metallic film. The gray (red online) solid circle in Fig. 6(a) marks the onset of this instability.

The void morphological response to increasing stress level Σ is characterized further in Figs. 6(b)–6(d). Specifically, the evolution of the maximum extent of the void sur-

face across the metallic thin film, $Y_{\max}(t)$, is depicted in three representative cases corresponding to increasing levels of Σ . Figure 6(b) shows $Y_{\max}(t)$, in the absence of mechanical stress ($\Sigma=0.0$), starting from a semicircular shape as the initial void morphology. Initially, the void attempts to reach a steady void morphology, resembling that of Fig. 5(c). This steady state, however, is unstable at $\Gamma=4.05$ as implied by Fig. 5(a) and the void morphology evolves to the stable time-periodic state as shown in Fig. 6(b). For $\Sigma=0.026 > \Sigma_c$, the initial void evolution is similar to that in Fig. 6(b). However, at this stress level, the applied mechanical stress suppresses the surface wave propagation and the time-periodic state is not stabilized. As a result, the time-periodic oscillations of Fig. 6(c) are damped after a transient period and the void morphology reaches a steady state. Figure 6(d) shows the void morphological evolution under an applied mechanical stress that is strong enough to cause the failure of the film. The transient dynamics is analogous to that of Fig. 6(c). Nevertheless, the corresponding asymptotic state (a steady state) is unstable and further void morphological evolution leads to film failure. Inset (ii) in Fig. 6(d) shows a snapshot from the void evolution near the failure of the film; the void tip is seen to have extended to almost touch the opposite edge of the film. The time to failure, $t=t_f$, is defined as the time required for the void tip to extend across y to the opposite edge of the film. As $t \rightarrow t_f$, the void morphology exhibits a logarithmic singularity expressed by $Y_{\max} \sim \ln(1-t/t_f)$. This linear dependence of Y_{\max} on $\ln(1-t/t_f)$ is demonstrated in inset (i) of Fig. 6(d). This scaling result is in agreement with the theoretical analysis of electromigration failure conducted by Mahadevan and Bradley.¹¹

Figure 7 shows representative results of the void morphological response when the current-driven system is acted on simultaneously by the applied mechanical stress for electric-field strength less than that at the $\Sigma=0.0$ Hopf point, $\Gamma=\Gamma_c$. In other words, we move along the Σ axis in the parameter space for $\Gamma=3.85$ ($\Gamma < \Gamma_c$), keeping the values of the other parameters (Λ , A , m , and ϕ) equal to those that yielded the bifurcation diagram in Fig. 5(a). The resulting dynamical response is summarized in the bifurcation diagram in Fig. 7(a) with Σ as the bifurcation parameter, $\varepsilon=\varepsilon(\Sigma)$. As Σ increases from $\Sigma=0$, a supercritical Hopf bifurcation occurs at $\Sigma=\Sigma_{c,1}$, marking the transition to a stable time-periodic response from a stable steady one. Further increase in the mechanical stress level Σ leads to another supercritical bifurcation at $\Sigma=\Sigma_{c,2}$ that marks the onset of transition from a stable time-periodic state to a stable steady state. This transition corresponds to a Hopf bifurcation at $\Sigma=\Sigma_{c,2}$ as the stress level decreases from higher values of Σ . This Hopf bifurcation also is supercritical, consistent with all the Hopf bifurcations occurring at this symmetry case, $m=2$.²² The supercritical nature of both Hopf bifurcations, at $\Sigma=\Sigma_{c,1}$ and at $\Sigma=\Sigma_{c,2}$, is confirmed by the quadratic polynomial fits to the parametric dependence, $\varepsilon=\varepsilon(\Sigma)$, of the stable time-periodic responses in the vicinity of both Hopf points, $\Sigma \rightarrow \Sigma_{c,1}^+$ ($\Sigma > \Sigma_{c,1}$) and $\Sigma \rightarrow \Sigma_{c,2}^-$ ($\Sigma < \Sigma_{c,2}$). The evolution of the maximum extent of the void surface across the metallic thin film, $Y_{\max}(t)$, is shown for four different cases: (i) toward a steady state at $\Sigma=0$, (ii) at a time-periodic state at $\Sigma_{c,1} < \Sigma=0.0013 < \Sigma_{c,2}$, (iii) toward a steady state at

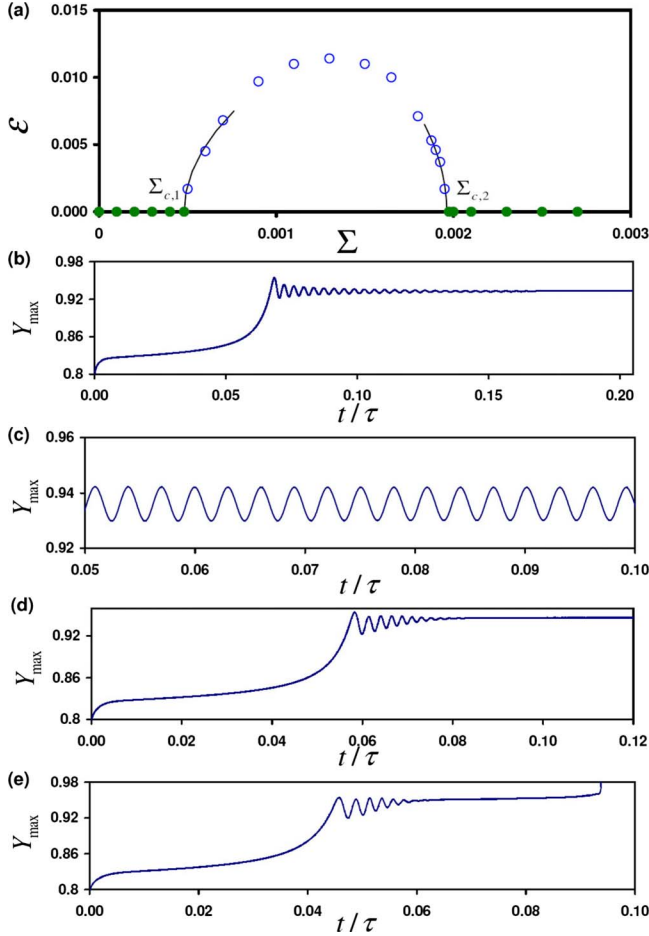


FIG. 7. (Color online) (a) Bifurcation diagram of the electromechanically driven surface morphological response of a void in a metallic thin film. The oscillation amplitude ε in the evolution of the maximum extent of the void surface across the film, Y_{\max} , is plotted at the asymptotic state as a function of the mechanical stress Σ . Open dark gray (blue online) and solid light gray (green online) circles denote time-periodic and steady states, respectively. The solid curves are quadratic polynomial fits to the parametric dependence of the stable time-periodic responses in the vicinity of the critical points, $\Sigma \rightarrow \Sigma_{c,1}^+$ and $\Sigma \rightarrow \Sigma_{c,2}^-$, respectively. The other parameter values are $\Gamma = 3.85$, $\Lambda = 0.80$, $A = 2.9$, $m = 2$, and $\phi = 45^\circ$. (b)–(d) Evolution of Y_{\max} toward or at the asymptotic states for $\Gamma = 3.85$ and (b) $\Sigma = 0.0$, (c) $\Sigma = 0.0013$, and (d) $\Sigma = 0.0025$. (e) Evolution of Y_{\max} at $\Gamma = 3.85$ and $\Sigma = 0.0029$. The corresponding asymptotic state (a steady state) is unstable and failure occurs by void-tip extension to reach the opposite edge of the film.

$\Sigma = 0.0025 > \Sigma_{c,2}$, and (iv) toward the instability that leads to film failure at $\Sigma = 0.0029$. These cases of void evolution are depicted in Figs. 7(b)–7(e), respectively. In all cases of Fig. 7, the characteristics of the void morphological evolution toward a stable time-periodic state and toward film failure are completely analogous to those discussed for the morphological responses depicted in Figs. 6(b)–6(d), respectively.

The void morphological evolution was simulated systematically with different parametric starting points, i.e., electric-field strength Γ , in the vicinity of the $\Sigma = 0$ Hopf point ($\Gamma = \Gamma_c$) in the bifurcation diagram in Fig. 7(a) and

increasing level of applied mechanical stresses Σ . Changes in the parametric starting point for the bifurcation analysis upon varying Σ resulted in different values of Σ_c , when the system is stressed at $\Gamma > \Gamma_c$, and different values of $\Sigma_{c,1}$ and $\Sigma_{c,2}$, when it is stressed at $\Gamma < \Gamma_c$. However, the qualitative response of the void morphology to the simultaneous action of the applied mechanical stress remained similar to that depicted in Fig. 6 for all $\Gamma > \Gamma_c$, and similar to that depicted in Fig. 7 for all $\Gamma < \Gamma_c$. The systematic analysis of the electromechanically driven response in this symmetry case, $m = 2$, was carried out over the broadest region of parameter space where time-periodic asymptotic states are found to be stable, well beyond the bifurcation analysis that resulted in the findings of Figs. 6 and 7. Some representative results are shown in Fig. 8 for parameter values $\Lambda = 0.80$, $A = 3.1$, $m = 2$, and $\phi = 45^\circ$. Figure 8(a) shows the corresponding bifurcation diagram with Γ as the bifurcation parameter, $\varepsilon = \varepsilon(\Gamma)$, at $\Sigma = 0$, while Fig. 8(b) shows the bifurcation diagram with Σ as the bifurcation parameter, $\varepsilon = \varepsilon(\Sigma)$, at $\Gamma = 3.85 > \Gamma_c$ at $\Sigma = 0.0$.

IV. SUMMARY AND CONCLUSIONS

Based on self-consistent dynamical simulations according to a realistic fully nonlinear model of surface morphological evolution, the occurrence of complex oscillatory asymptotic states was investigated for electromechanically driven void surfaces in thin films of fcc metals with $\langle 110 \rangle$ - and $\langle 100 \rangle$ -oriented film planes. A systematic bifurcation analysis with the level of the applied biaxial tensile stress as the bifurcation parameter over a range of applied electric-field strengths and given surface diffusional anisotropy parameters was carried out. For $\langle 110 \rangle$ -oriented film planes, $m = 1$, the analysis revealed that upon increasing the level of the applied mechanical stress a transition occurs from morphologically stable steady states to morphologically stable time-periodic states; this transition corresponds to a subcritical Hopf bifurcation. Most importantly, the analysis predicted a period-doubling-bifurcation route to chaos upon further increase in the applied stress level. Over the parameter range examined, two chaotic regimes were predicted that are separated by a periodic window; the system exits the first chaotic regime to a 3-cycle and enters the second one through another sequence of period-doubling bifurcations. The corresponding strange attractors, i.e., the chaotic asymptotic states in the doubly driven void morphological evolution, were characterized over the parameter range that was examined.

It should be emphasized that the observed chaotic dynamics and the period-doubling-bifurcation route to chaos are characteristic of the low symmetry, $m = 1$, of the surface diffusional anisotropy, which makes the Hopf bifurcation that destabilizes the original steady state subcritical. For $\langle 100 \rangle$ -oriented film planes, $m = 2$, the $\Sigma = 0$ Hopf bifurcation upon increasing Γ is supercritical. It was demonstrated that Hopf bifurcation also occurs at $m = 2$ upon varying Σ for $\Sigma > 0$. These Hopf bifurcations were found to be supercritical, marking the onset of transition from stable steady states to stable time-periodic states. These supercritical Hopf bifurcations do not set the electromechanically driven void surface morphology on a route to chaos. Instead, for $m = 2$, in-

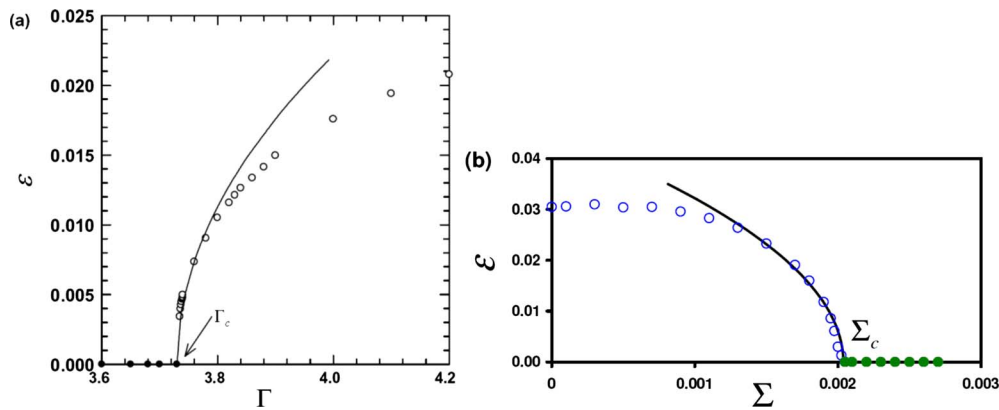


FIG. 8. (Color online) Bifurcation diagrams of the electromechanically driven surface morphological response of a void in a metallic thin film. The oscillation amplitude ε in the evolution of the maximum extent of the void surface across the film, Y_{\max} , is plotted at the asymptotic state as a function of (a) the electric-field strength Γ at $\Sigma=0$ (taken from Ref. 22) and (b) the mechanical stress level Σ at $\Gamma=3.85$. The other parameter values are $\Lambda=0.80$, $A=3.1$, $m=2$, and $\phi=45^\circ$. In both (a) and (b), solid and open circles represent stable steady and time-periodic states, respectively. In both cases, the solid curves are quadratic polynomial fits to the corresponding parametric dependences of the stable time-periodic responses in the vicinity of the Hopf bifurcation points.

creasing Σ starting from a time-periodic state suppresses the oscillatory surface dynamics and leads the void morphology to a stable steady state; this steady state is stable up to high enough stress levels that cause film failure through void-tip extension.

Chaotic behavior is not common in the diffusional dynamics of solid materials. In the system of interest in this study, namely, the electromigration-driven dynamics of voids in metallic thin films as simulated by the model of Sec. II, the discovery of stable chaotic asymptotic states is intriguing. In this system, without the simultaneous action of mechanical stress, no period-doubling bifurcation or chaos has been found over the broadest region of parameter space examined for either case $m=1$ or 2 in the symmetry of surface diffusional anisotropy.²² Moreover, at the highest relevant case of symmetry corresponding to $\langle 111 \rangle$ -oriented film planes, $m=3$, it has not been possible to stabilize even time-periodic asymptotic states.²¹ Only under the simultaneous action of mechanical stress and only at low symmetry of surface diffusional anisotropy, $m=1$, the stabilization of chaotic attractors has been possible; this has been the outcome of a systematic exploration of parameter space with biaxial tension as the mechanical loading mode. Nevertheless, it should be mentioned that, in the case of electromigration-driven oscillatory shape evolution of epitaxial islands,¹⁸ it was found based on kinetic Monte Carlo simulations that the propensity for complex dynamical behavior decreases as the number of symmetry axes is reduced.³⁰ This interesting qualitative difference between this dynamical response and the complex void dynamics in our study can be attributed to the existence of high stress and electric-field concentrations at the upper edge of the voids that are confined in the narrow metallic thin films addressed in our study; such high external field concentrations are not observed in the epitaxial-island systems.

As mentioned in Sec. II, the model employed in this study is a physical model that has been validated quite well by meticulous comparisons of its predictions with the entire set of experimental measurements and observations on this system that are available in the literature. These comparisons include electromigration-driven void surface morphological evolution,^{8,15} void morphological instabilities resulting in the formation of stress-induced cracks emanating from electromigration-induced slits,^{10,15} and electrical resistance evolution in metallic interconnect lines,¹⁹ including quantitative agreement of our modeling predictions²² with the only experimental measurement that has been reported of a stable time-periodic state in the evolution of electrical resistance.³¹ To the best of our knowledge, controlled experiments of electromigration-driven void evolution in metallic thin films under the simultaneous action of mechanical stress have not been reported to date. Nevertheless, we hope that our study will motivate systematic protocols of such controlled experiments that will confirm our modeling predictions.

The results of our bifurcation analysis have shed light into the complex dynamics of void surfaces in metallic thin films under the combined action of applied electric fields and mechanical stresses. Moreover, the results imply that current-driven void dynamical responses in thin films can be controlled through proper tailoring of the film properties (such as texture or film-plane crystallographic orientation) that determine surface diffusional anisotropy and the electromechanical conditions (strength of applied electric field and level of applied or residual biaxial tensile stress).

ACKNOWLEDGMENT

This work was supported by the Office of Basic Energy Sciences, U.S. Department of Energy through Grant No. DE-FG02-07ER46407.

*Corresponding author; maroudas@ecs.umass.edu

- ¹J. Krug and H. T. Dobbs, Phys. Rev. Lett. **73**, 1947 (1994).
- ²D. Maroudas, Appl. Phys. Lett. **67**, 798 (1995).
- ³M. Mahadevan and R. M. Bradley, J. Appl. Phys. **79**, 6840 (1996).
- ⁴M. Schimschak and J. Krug, Phys. Rev. Lett. **78**, 278 (1997).
- ⁵L. Xia, A. F. Bower, Z. Suo, and C. F. Shih, J. Mech. Phys. Solids **45**, 1473 (1997).
- ⁶M. Schimschak and J. Krug, Phys. Rev. Lett. **80**, 1674 (1998).
- ⁷M. R. Gungor and D. Maroudas, Appl. Phys. Lett. **72**, 3452 (1998); Surf. Sci. **415**, L1055 (1998).
- ⁸M. R. Gungor and D. Maroudas, J. Appl. Phys. **85**, 2233 (1999).
- ⁹D. R. Fridline and A. F. Bower, J. Appl. Phys. **85**, 3168 (1999).
- ¹⁰M. R. Gungor, D. Maroudas, and L. J. Gray, Appl. Phys. Lett. **73**, 3848 (1998); M. R. Gungor and D. Maroudas, Surf. Sci. **432**, L604 (1999).
- ¹¹M. Mahadevan and R. M. Bradley, Phys. Rev. B **59**, 11037 (1999).
- ¹²R. M. Bradley, Phys. Rev. E **60**, 3736 (1999).
- ¹³M. Schimschak and J. Krug, J. Appl. Phys. **87**, 695 (2000).
- ¹⁴M. R. Gungor and D. Maroudas, Surf. Sci. **461**, L550 (2000); J. S. Cho, M. R. Gungor, and D. Maroudas, *ibid.* **575**, L41 (2005).
- ¹⁵M. R. Gungor and D. Maroudas, Int. J. Fract. **109**, 47 (2001).
- ¹⁶R. M. Bradley, Phys. Rev. E **65**, 036603 (2002).
- ¹⁷J. S. Cho, M. R. Gungor, and D. Maroudas, Appl. Phys. Lett. **85**, 2214 (2004); M. R. Gungor and D. Maroudas, J. Appl. Phys. **101**, 063513 (2007).
- ¹⁸P. Kuhn, J. Krug, F. Hausser, and A. Voigt, Phys. Rev. Lett. **94**, 166105 (2005).
- ¹⁹J. S. Cho, M. R. Gungor, and D. Maroudas, Appl. Phys. Lett. **86**, 241905 (2005); **88**, 221905 (2006); J. Appl. Phys. **101**, 023518 (2007).
- ²⁰M. Dufay, J.-M. Debierre, and T. Frisch, Phys. Rev. B **75**, 045413 (2007).
- ²¹E. D. Koronaki, M. R. Gungor, C. I. Siettos, and D. Maroudas, J. Appl. Phys. **102**, 073506 (2007).
- ²²J. S. Cho, M. R. Gungor, and D. Maroudas, Surf. Sci. **602**, 1227 (2008).
- ²³R. M. Bradley, Appl. Phys. Lett. **93**, 213105 (2008).
- ²⁴V. Tomar, M. R. Gungor, and D. Maroudas, Phys. Rev. Lett. **100**, 036106 (2008); Appl. Phys. Lett. **92**, 181905 (2008); **94**, 181911 (2009).
- ²⁵O. Kraft and E. Arzt, Acta Mater. **45**, 1599 (1997).
- ²⁶A. I. Sauter and W. D. Nix, IEEE Trans. Compon., Hybrids, Manuf. Technol. **15**, 594 (1992).
- ²⁷L. J. Gray, D. Maroudas, and M. N. Enmark, Comput. Mech. **22**, 187 (1998).
- ²⁸G. L. Baker and J. P. Gollub, *Chaotic Dynamics: An Introduction* (Cambridge University Press, Cambridge, England, 1990).
- ²⁹G. Iooss and D. D. Joseph, *Elementary Stability and Bifurcation Theory* (Springer-Verlag, New York, 1997).
- ³⁰M. Rusanen, P. Kuhn, and J. Krug, Phys. Rev. B **74**, 245423 (2006).
- ³¹S. Shingubara, H. Kaneko, and M. Saitoh, J. Appl. Phys. **69**, 207 (1991).